Effect of Lewis acid on catalytic dehydration of a chitin-derived sugar alcohol

Takuya Sagawa[a,b], Hirokazu Kobayashi[a,*], Atsushi Fukuoka [a,*]

[a]Institute for Catalysis, Hokkaido University, Kita 21 Nishi 10, Kita-ku, Sapporo, Hokkaido 001-0021, Japan.

[b]Department of Industrial Chemistry, Faculty of Science, Tokyo University of Science, 12-1 Ichigayafunagawara-machi, Shinjuku-ku, Tokyo, 162-0826, Japan.

*Corresponding author.

E-mail: kobayashi.hi@cat.hokudai.ac.jp (H.K.); fukuoka@cat.hokudai.ac.jp (A.F.)

Fax: +81-11-706-9139

Abstract

Chitin is an abundant marine biomass consisting of *N*-acetylglucosamine (NAG) units. NAG is a source for 2-acetamide-2-deoxyisosorbide (ADI), a condensed five-membered ring compound potentially useful for producing nitrogen-containing polymers. The synthetic route of ADI from NAG consists of hydrogenation of NAG to 2-acetamide-2-deoxysorbitol (ADS) by a supported metal catalyst and subsequent dehydration reaction by a Brønsted acid catalyst. However, the dehydration step has remained a challenge due to low reactivity of the substrate and low selectivity. Here, we report a combination of Brønsted acid and Lewis acid catalysts for accelerating the ADS dehydration. The additional use of a catalytic amount of ytterbium triflate in the ADS dehydration by trifluoromethanesulfonic acid catalyst shortens the reaction time by one third and moreover increases the yield of ADI by changing regio-selectivity of the reaction. Mechanistic roles of the ytterbium complex are discussed based on the experimental evidences and density functional theory calculations.

Keywords: chitin • acid-catalyzed dehydration • Lewis acid • homogeneous catalysis • 2-acetamide-2-deoxyisosorbide

1. Introduction

Chitin is a prominent marine biomass annually occurring in a scale of 10^{11} ton [1]. Shell waste of crustaceans such as crabs and shrimps are ready source for chitin, practically used in industries. This compound is a pure polymer of *N*-acetylglucosamine (NAG), which is a nitrogen-containing sugar, and can be degraded into the monomer unit by hydrolysis reactions (Figure 1) [2–5]. These facts make chitin an attractive potential feedstock for the production of organonitrogen compounds as typified by polymers and medicines [6,7]. Conversion of biomass to organonitrogen compounds has been attracting a significant attention in recent years [8–10], and use of chitin is a straightforward way to implement the nitrogen-containing biorefinery.

Chemical transformation of NAG has given several organonitrogen compounds that may be useful in polymer and pharmaceutical industries [11–20]. Among them, we focus on 2-acetamide-2-deoxyisosorbide (ADI), which has a condensed five-membered ring and a hydroxy and an acetamide groups that are suited for producing nitrogen-containing polymers (Figure 1) [20]. The structure of ADI is similar to that of isosorbide, a precursor to the polycarbonate named Durabio that shows remarkable mechanical strength and thermal stability due to its rigid structure [21]. As an analogy, we can expect that introduction of ADI units in polymers would impart good mechanical strength and heat resistance to the products.

ADI is synthesized *via* hydrogenation of NAG to 2-acetamide-2-deoxysorbitol (ADS) and subsequent two-step dehydration (Figure 1). Brønsted acids catalyze the dehydration reaction and first produce 1,4-, 3,6- and 1,5-anhydro-ADS. Among them, 1,4- and 3,6-anhydro-ADS undergo further dehydration to ADI, whereas 1,5-anhydro-ADS is a by-product. This reaction pathway is analogous to the production of isosorbide consisting of the hydrogenation of glucose to sorbitol followed by the dehydration of sorbitol (Figure S1). The structures of ADS and sorbitol are similar, but the dehydration of ADS is much slower than that of sorbitol. DFT calculations have revealed that the O atom in the acetamide group in ADS molecule traps an acid proton due to its basicity, thus leading to a high activation energy in the dehydration reaction [20]. This issue imposes a high temperature and a long reaction time to complete the dehydration of ADS. Moreover, this reaction produces a large amount of 1,5-anhydro-ADS, *viz.* low regio-selectivity toward the formation of desired intermediates. As a

result, the maximum yield of ADI has been limited to 33% so far [high-performance liquid chromatography (HPLC) yield] [20].

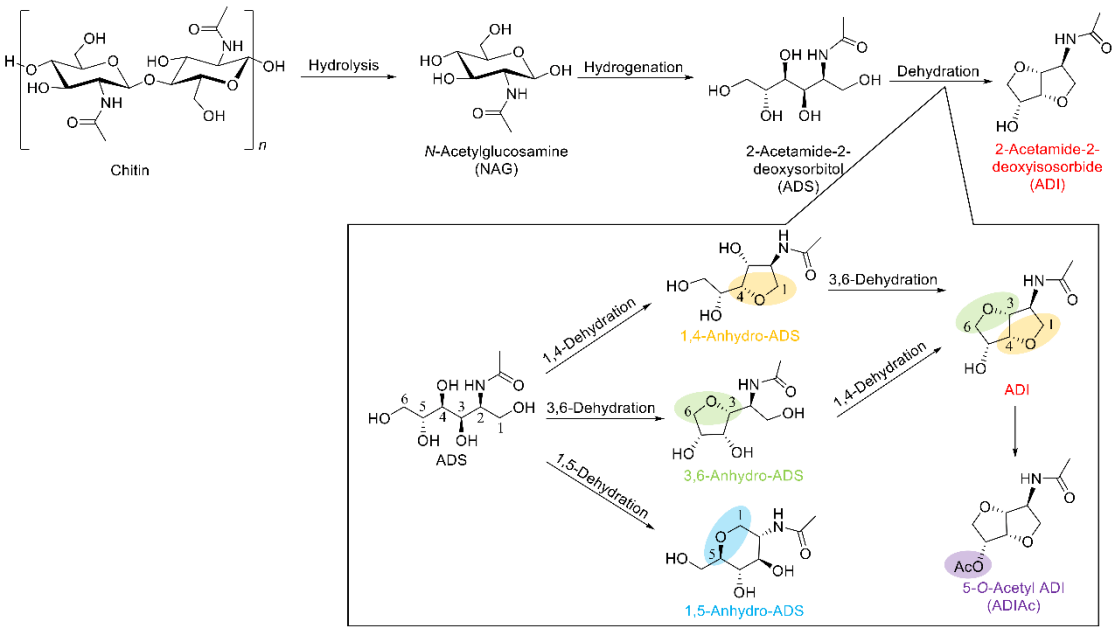

Figure 1. Synthetic route of ADI from chitin.

The objective of this work is to improve efficiency of the ADI synthesis, for which we add a Lewis acid in the ADS dehydration catalyzed by a Brønsted acid. We hypothesize that a Lewis acid coordinates amide O atoms, thus inhibiting trap of acid protons by the same site. Especially, rare earth triflates have strong Lewis acidity derived from electron-deficient metal cations [22] that coordinate carbonyl O. Indeed, this property has been applied for promoting several catalytic reactions as follows: Dobereiner and coworkers reported that Pd-catalyzed cross-coupling of amides and aryl halides is accelerated by metal triflate co-catalysts [23]. Fu and coworkers represented the promotion of hydrogenolysis of lactones to carboxylic acids using a metal triflate [24]. Additionally, it has been found that the regio-selectivity in the dehydration reactions of sugar alcohols strongly relies on specific structures of the substrates [25,26]. Thus, the coordination of Lewis acid on ADS possibly changes the selectivity. With this idea, this work demonstrates the acceleration of the dehydration of ADS by adding rare earth triflates and proposes possible roles of the Lewis acids based on the experimental

results and density functional theory (DFT) calculations.

2. Experimental

2.1. Materials

NAG, diethyl ether (Et_2O) and distilled water were purchased from FUJIFILM Wako Pure Chemical Corporation. Lutetium (III) trifluoromethanesulfonate [$Lu(OTf)_3$], $Er(OTf)_3$ and $La(OTf)_3$ were obtained from Aldrich. HOTf, $Yb(OTf)_3$, $Tm(OTf)_3$ and $Sc(OTf)_3$ were purchased from Tokyo Chemical Industry. ADS was prepared from NAG as reported previously [20].

2.2. Conversion of ADS by acid catalysts

HOTf was dissolved in Et_2O (1 mL) in a two-necked egg-plant flask (borosilicate glass, 100 mL), and then a mixture of ADS (1.00 mmol) and a Lewis acid was added into the solution. After removing Et_2O under reduced pressure, the apparatus was equipped with a Teflon-coated thermocouple (ø1.6 mm) and a condenser connected to a rotary pump, and put into an oil bath to keep the reaction temperature at 150 °C for a designated time. After cooling down the glass reactor, water (20 mL) was added to the mixture to analyze soluble products by a high-performance liquid chromatograph (HPLC; Shimadzu, Prominence) equipped with a RPM-Monosaccharide Pb++ column (Phenomenex, mobile phase: water 0.6 mL min^{-1}, 70 °C) and a refractive index detector. Product yield was calculated by an absolute calibration method (error < 0.3%). Product yield is shown in mole basis to keep yield value unchanged in the presence or absence of acetyl groups. Reproducibility of the reactions was confirmed at a typical reaction condition three times (error < 2%). 5-*O*-acetyl-ADI (ADIAc) was isolated from a reaction mixture by the HPLC fraction collection (retention time 19.8 min).

2.3. Characterization

Nuclear magnetic resonance (NMR) spectra were recorded on an ECX-600 spectrometer (JEOL). ^1H NMR (600 MHz), proton decoupled ^{13}C NMR (151 MHz), distortional enhancement by polarization transfer (DEPT), ^{13}C–^1H heteronuclear multiple quantum coherence (HMQC), and ^{13}C–^1H heteronuclear multiple bond correlation (HMBC) spectra were measured using 4,4-dimethyl-4-

silapentane-1-sulfonic acid sodium salt (DSS) as an external standard. Low-resolution electrospray ionization mass spectra (LR-ESI MS) were recorded on a Shimadzu LCMS-2020 system attached with a Synergi Hydro-RP column.

ADIAc: ^{1}H NMR (600 MHz, $CDCl_3$): δ = 1.97 (s, 3H, NHCOC*H*$_3$), 2.11 (s, 3H, OCOC*H*$_3$), 3.82 (d, *J* = 9.6 Hz, 1H, C1–*H*), 3.84 (dd, *J* = 4.9, 10.3 Hz, 1H, C6–*H*), 3.88 (dd, *J* = 5.5, 10.3 Hz, 1H, C6–*H*), 3.92 (dd, *J* = 4.1, 9.6 Hz, 1H, C1–*H*), 4.38 (d, *J* = 4.8, 1H, C3–*H*), 4.44 (dd, *J* = 4.1, 7.5 Hz, 1H, C2–*H*), 4.74 (dd, *J* = 4.8, 4.8 Hz, 1H, C4–*H*), 5.12 (dd, *J* = 4.8, 5.5 Hz, 1H, C5–*H*), 5.87 (d, *J* = 7.5 Hz, 1H, N*H*). ^{13}C NMR (151 MHz, $CDCl_3$): δ = 20.6, 23.1, 56.2, 70.7, 73.0, 74.0, 80.3, 86.6, 169.7, 170.4. LRMS (LR-ESI-TOF) *m*/*z* calcd. for $C_7H_{14}NO_6$ $[M+H]^+$ 230; found 230.

2.4. Theoretical calculations

DFT calculations were performed using the Gaussian 16 (revision A.03) software at the unrestricted open shell B3LYP/def2-TZVPP/6-311+G(d,p)//B3LYP/def2-SVP/6-31G(d) level of theory, where the Karlsruhe basis sets were applied for metal elements with the effective core potential (def2-ECP) and the Pople ones were chosen for all the other elements [27–30]. We used the fine grid with a 10-digit accuracy for numerical integration to reduce the calculation time. Solvation effect was taken into account by SMD, for which MeOH was used as a solvent model instead of ADS [31].

Gibbs free energy of a structure at 298 K was obtained by the Gaussian's freq option giving $H°$, $S°_{trans.}$, $S°_{rot.}$, $S°_{vib.}$ and $S°_{elec.}$, and the accuracy was improved by eqs. 1–4 for the liquid-phase reaction as follows: the pV term in enthalpy ($H = U + pV$) can be approximated to 0 in liquid phase, thus subtracting $p°V_{gas}$ from the calculated enthalpy for gas phase (eq. 2). The translational entropy was corrected by the free volume theory (eq. 3) [32], where a free volume (V_{free}) was approximately obtained by the cavity volumes calculated based on van der Waals radius at electrostatic scaling factors (α) of 1.0 and 1.2 (eq. 4) [33]. Gaussian provided the cavity volume for one molecule system in the presence of the self-consistent reaction field (SCRF) option with specifying α value, and the Avogadro constant was multiplied to be mole basis.

$$G° = H°_{rev.} - T(S°_{trans,rev.} + S°_{rot.} + S°_{vib.} + S°_{elec.}) \quad (1)$$

$H°_{rev.} = H° - p°V_{gas}$ (2)

$S°_{trans,rev.} = S°_{trans.} + R(\ln V_{free} - \ln V_{gas})$ (3)

$V_{free} = (V_{\alpha=1.2}{}^{1/3} - V_{\alpha=1.0}{}^{1/3})^3$ (4)

$Yb(OTf)_3$, the main catalyst used in this work, accepts the coordination of multiple ADS molecules [e.g., $Yb(OTf)_3(ADS)_2$], but DFT calculations for this system is time consuming. Instead, we replaced one ADS molecule with ethylene glycol (EG) to reduce the calculation cost. For the transition state calculations, the structure of $Yb(OTf)_3$(ADS)(EG) was optimized in advance, and afterward $Yb(OTf)_3$(EG) moiety was frozen during the calculation of reactions occurring on ADS in the complex; otherwise, the structural optimization seldom converged. Atomic coordinates at the transition states are shown in Supporting Information (Tables S1–S4). We found the presence of only one imaginary frequency vibration and the intrinsic reaction coordinate (IRC) [34] connecting expected substrate and product.

3. Results and discussion

3.1. Catalytic reactions

We performed the dehydration of ADS in the presence of HOTf (Brønsted acid) at a substrate/catalyst (S/C) mole ratio of 2 and rare earth—La, Er, Tm, Yb, Lu, Sc—triflates (Lewis acid) at a S/C ratio of 10 under neat condition with decreased pressure below 0.1 kPa at 150 °C for one hour (Table 1). A controlled experiment without a Lewis acid gave >99% conversion of ADS, and the products were ADI (22% yield), mono-anhydro-ADS (21% in total) and 5-*O*-acetyl ADI (ADIAc; 9.1% yield) (entry 1). ADIAc is a newly identified product in this work, using NMR techniques and MS analysis (Figures S2–S6). The presence of ADIAc indicates the formation of some deacetylated product as a counterpart, which is supported by the MS analysis that has detected deacetylated ADS ($[M+H]^+$, m/z = 182) and deacetylated mono-anhydro-ADS ($[M+H]^+$, m/z = 164). The deacetylated products and unidentified compounds such as humins are denoted “others” in the table (48%). Addition of metal triflates increased the yield of ADI in different degrees (32–40%; entries 2–7), and the difference likely correlated with the Lewis acid strength, in other words oxophilicity, of each triflate (Figure S7). Table

1 provides the relative oxophilicity of metal triflates determined by an MS technique [35] in addition to the catalytic results. $La(OTf)_3$, having the lowest oxophilicity, slightly increased the yield of ADI (32%; entry 2). More oxophilic triflates (Er^{3+}, Tm^{3+}, Yb^{3+} and Lu^{3+}) were more promising for this reaction (entries 3–5, 7), among which $Yb(OTf)_3$ gave the highest yield of ADI (40%). Further increase in oxophilicity was less meaningful, as $Sc(OTf)_3$ gave a similar or lower yield of ADI (37%; entry 8), compared to $Yb(OTf)_3$. It is also notable that addition of any triflates decreased the yield of 1,5-anhydro-ADS from 17% to 4.7–9.7% and that of ADIAc from 9.1% to 0.8–2.2%, which contributed to the improvement of ADI yield. Effect of triflates on product selectivity is discussed later in more detail. Based on these results, $Yb(OTf)_3$, possessing the second highest oxophilicity among the triflates tested, was chosen for further study. We have found that $Yb(OTf)_3$ is not very active in the absence of HOTf (entry 6), and therefore the combination of HOTf and $Yb(OTf)_3$ is effective.

Table 1. Dehydration of ADS using HOTf and metal triflate.[a]

Entry	Lewis acid	Oxophilicity[b]	Conv. /%	Yield of product[c] /%					
				1,4-AHADS[d]	3,6-AHADS[d]	1,5-AHADS[d]	ADI	ADIAc	Others
1	None	–	>99	1.4	2.4	17	22	9.1	48
2	$La(OTf)_3$	1.40	>99	0.9	1.5	9.7	32	2.2	54
3	$Er(OTf)_3$	1.43	>99	0.1	0.7	5.1	38	0.9	55
4	$Tm(OTf)_3$	1.45	>99	0.1	1.2	6.2	36	1.5	55
5	$Yb(OTf)_3$	1.52	>99	0.1	0.8	6.0	40	0.8	52
6[e]	$Yb(OTf)_3$	1.52	>99	24	3.1	32	4.7	2.9	33
7	$Lu(OTf)_3$	1.42	>99	0.1	1.1	6.8	36	1.3	55
8	$Sc(OTf)_3$	1.55	>99	0.1	1.2	4.7	37	0.8	56

[a]Reaction conditions: ADS 223 mg (1.00 mmol), HOTf 75 mg (0.50 mmol, S/C = 2.0), Lewis acid (0.10 mmol, S/C = 10), no solvent, 150 °C, 1 h, < 0.1 kPa. [b]Relative oxophilicity.[17] [c]Mole of

product/mole of ADS, except for Others (100% − yield of identified products). [d]Anhydro-ADS. [e]No HOTf.

We studied effect of reaction conditions on the dehydration of ADS in the presence of HOTf and $Yb(OTf)_3$. First, the concentration of $Yb(OTf)_3$ is critical to increase the yield of ADI (Table 2). Low concentrations of $Yb(OTf)_3$ (S/C = 50 and 20) gave minor influence on the ADI yield (23% and 25%, respectively; entries 10, 11), compared to the reaction in the absence of $Yb(OTf)_3$ (22% yield, entry 9). Increase in the amount to S/C = 10 and 5 provided ADI in good yields of 40% and 36%, respectively (entries 12, 13). A larger amount of $Yb(OTf)_3$ rather decreased the yield to 25% at S/C = 2 (entry 15). In this case, 1,4-anhydro-ADS and 3,6-anhydro-ADS still remained in 8.1% yield in total, thus indicating that too much $Yb(OTf)_3$ slows down the dehydration reactions. This inhibition effect might be due to the coordination of $Yb(OTf)_3$ not only on the amide group of ADS and anhydro-ADS but also on their terminal OH groups, namely the sites where protons should bind for the dehydration reactions. To assess this possibility, DFT calculations determined the binding energy of ADS on $Yb(OTf)_3$(EG) complex, in which EG was employed for the convenience (see Experimental). The binding Gibbs free energies ($\Delta G°$) for the amide group and the C1–OH group were −5.9 and −3.5 kJ mol^{-1}, respectively, which were similar (Figure 2). Therefore, it is reasonable that excess $Yb(OTf)_3$ leads to its coordination onto the OH groups in terms of the equilibrium theory [$K = \exp(-\Delta G°/RT)$]. Another important fact is that lanthanoid accepts up to nine-coordination in the first coordination shell [36–38], which indicates that multiple ADS and product molecules can bind on a $Yb(OTf)_3$ complex. Thus, compared to the S/C ratio for $Yb(OTf)_3$, a few times larger amount of substrates may bind on $Yb(OTf)_3$. Hence, addition of $Yb(OTf)_3$ at an S/C ratio between 5 to 10 is the most effective in this reaction.

Table 2. Effect of $Yb(OTf)_3$ concentration on the ADS dehydration.[a]

Entry	$Yb(OTf)_3$ S/C	Conv. /%	Yield of product[b] /%					
			1,4-AHADS[c]	3,6-AHADS[c]	1,5-AHADS[c]	ADI	ADIAc	Others
9	∞	>99	1.4	2.4	17	22	9.1	49
10	50	>99	0.2	1.3	13	23	5.1	58
11	20	>99	0.9	1.5	9.7	25	3.1	60
12	10	>99	0.1	0.8	6.0	40	0.8	53
13	5	>99	0.1	0.7	5.1	36	1.0	56
14	2.5	>99	2.9	1.9	5.3	31	1.2	57
15	2	>99	5.2	2.9	5.7	25	1.2	61

[a]Reaction conditions: ADS 223 mg (1.00 mmol), HOTf 75 mg (0.50 mmol, S/C = 2.0), no solvent, 150 °C, 1 h, < 0.1 kPa. [b]Mole of product/mole of ADS, except for Others (100% − yield of identified products). [c]Anhydro-ADS.

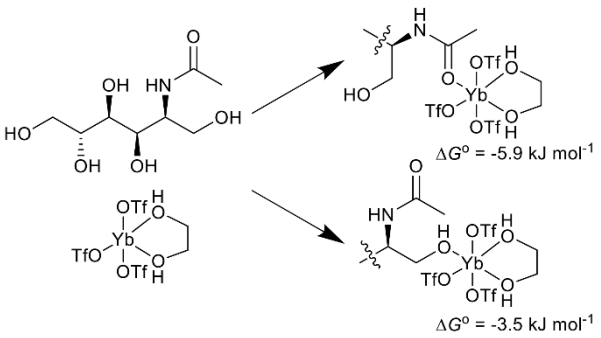

Figure 2. Gibbs free energies for coordination of ADS on $Yb(OTf)_3(EG)$ estimated by the DFT calculations.

For the temperature effect, a reaction temperature as low as 130 °C gave ADI in 31% yield and ADIAc in 4.0% yield with the formation of by-products (1,5-anhydro-ADS 11%, others 52%) (Table

3, entry 16). Increase in the temperature to 150 °C improved the yield of ADI to 40%, while decreasing yields of 1,5-anhydro-ADS and ADIAc (entry 18). The reduction in ADIAc yield is possibly due to conversion of ADIAc to ADI as discussed later. Further increase in temperature led to the formation of unidentified by-products (Others 59% at 170 °C, entry 20). Accordingly, the optimal reaction temperature was 150 °C for the production of ADI.

Table 3. Effect of reaction temperature on the ADS dehydration.[a]

Entry	Temp. /°C	Conv. /%	Yield of product[b] /%					
			1,4-AHADS[c]	3,6-AHADS[c]	1,5-AHADS[c]	ADI	ADIAc	Others
16	130	>99	1.4	1.2	11	31	4.0	52
17	140	>99	1.3	1.6	8.7	33	4.1	51
18	150	>99	0.1	0.8	6.0	40	0.8	53
19	160	>99	0.1	0.6	4.4	38	1.1	56
20	170	>99	0.1	0.4	2.5	36	1.0	59

[a]Reaction conditions: ADS 223 mg (1.00 mmol), HOTf 75 mg (0.50 mmol, S/C = 2.0), $Yb(OTf)_3$ 62 mg (0.10 mmol, S/C = 10), no solvent, 1 h, < 0.1 kPa. [b]Mole of product/mole of ADS, except for Others (100% − yield of identified products). [c]Anhydro-ADS.

We compared the time courses of ADS dehydration in the presence and absence of $Yb(OTf)_3$ to clarify more detailed roles of $Yb(OTf)_3$ in the reaction. The reaction without $Yb(OTf)_3$ (Figures 3a,b) consumed ADS completely at 5 min, and produced 1,4-anhydro-ADS (10%), 3,6-anhydro-ADS (11%) and 1,5-anhydro-ADS (14%). Afterward, yield of ADI continuously increased over 180 min, and the maximum yield of ADI was 32%, almost the same as our previous report [6]. Additionally, ADIAc was produced in 9.1% yield at 60 min in parallel with ADI. In the presence of $Yb(OTf)_3$ (Figures 3c,d), ADS was mostly consumed at 5 min, which was similar to the reaction without $Yb(OTf)_3$. However, it is notable that $Yb(OTf)_3$ changed the product distribution among mono-anhydro-ADS: decreasing

1,4-anhydro-ADS (6.4% yield) and 1,5-anhydro-ADS (4.4%) but increasing 3,6-anhydro-ADS (15%). Namely, $Yb(OTf)_3$ enhances the dehydration at C6 position (3,6-dehydration) over that at C1 position (1,4- and 1,5-dehydration), perhaps by binding on ADS. This change in regio-selectivity is useful to decrease the formation of 1,5-anhydro-ADS, a major by-product. Moreover, $Yb(OTf)_3$ accelerated the dehydration of mono-anhydro-ADS to ADI, completing the formation of ADI at 60 min with an improved yield of 40%. It was not straightforward that the yield of ADI slightly increased after 30 min, when 1,4- and 3,6-anhydro-ADS had already been consumed. We speculate that the acetyl group of ADIAc transfers to deacetylated products to produce two molecules of ADI at maximum in the duration. As mentioned above, the MS analysis has detected deacetylated precursors for ADI production.

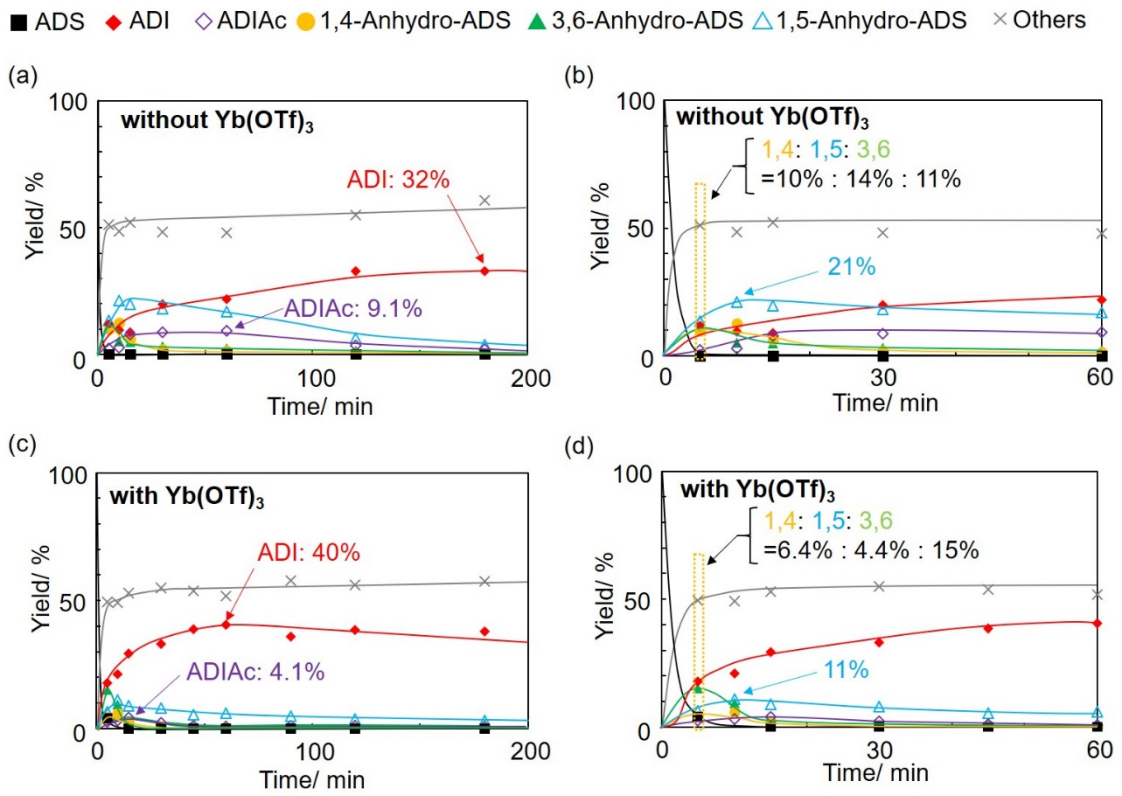

Figure 3. Time courses of ADS dehydration reactions at 150 °C: (a) in the absence of $Yb(OTf)_3$, (b) an enlarged image of (a), (c) in the presence of $Yb(OTf)_3$, (d) an enlarged image of (c).

3.2. Energy diagrams for ADS dehydration

We employed DFT calculations to clarify the roles of $Yb(OTf)_3$ in this reaction system. $Yb(OTf)_3$(ADS)(EG) complex was used as a starting structure for calculating all reactions for convenience as mentioned above.

Our initial hypothesis in this work was that coordination of $Yb(OTf)_3$ on the amide O atom of ADS may prevent the strong binding of proton on the same O atom. In the DFT calculations, free ADS underwent protonation of the amide O atom at a ΔE (sum of electronic and zero-point vibration energies) of −76 kJ mol^{-1} (Figure 4, i), whereas the ADS within $Yb(OTf)_3$(ADS)(EG) did at −39 kJ mol^{-1} (ii-1). Consequently, the complexation of ADS successfully weakened the basicity of amide group, leading the complex to favor the protonation of hydroxy groups (−41 kJ mol^{-1}; ii-2), similar to sorbitol (−43 kJ mol^{-1}; iii).

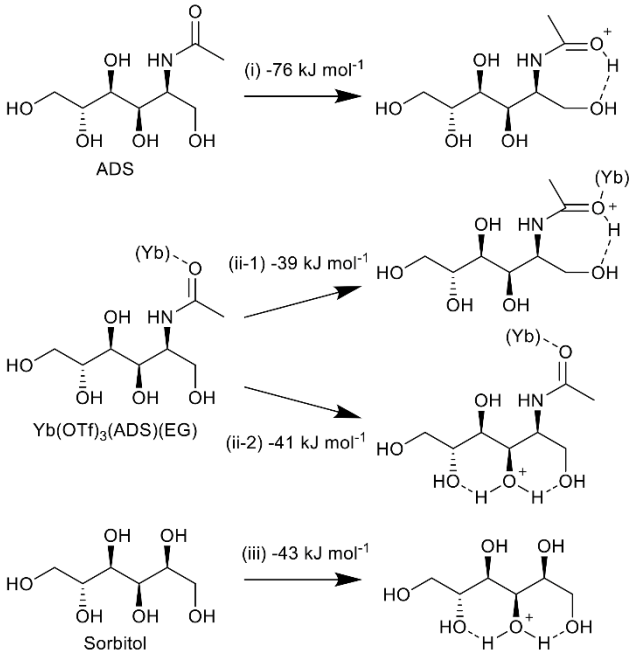

Figure 4. Protonation energies for ADS and sorbitol. The value includes electronic energy and zero-point vibration energy. (Yb) in structures indicates $Yb(OTf)_3$(EG).

We calculated energy diagrams for the 3,6-dehydration of ADS, the preferred reaction after the addition of $Yb(OTf)_3$. The most stable protonated forms of free ADS (Figure 5, blue line) and

$Yb(OTf)_3$(ADS)(EG) (red line) transfer protons onto C6–OH to be precursors for 3,6-dehydration, climb the potential energy surfaces to reach the transition states (TS), and eventually give protonated 3,6-anhydro-ADS and water. While the complexation of ADS with Yb lifted the large energy drop in protonation found for free ADS (−41 kJ mol^{-1} vs −76 kJ mol^{-1}), it only slightly increased the potential energy at the TS to +44 kJ mol^{-1} from +39 kJ mol^{-1} for free ADS. Thereby, $Yb(OTf)_3$(ADS)(EG) offered an apparent activation energy 30 kJ mol^{-1} lower than that given by free ADS.

Finally, we compared how much the coordination of ADS to Yb center changes potential energy at the TS in the 1,4- and 3,6-dehydration reactions. The complexation elevated the potential energy by 5 kJ mol^{-1} for the 3,6-dehydration (Figure 5; 44 − 39 = 5) and 8 kJ mol^{-1} for the 1,4-dehydration (Figure S8). Their difference (3 kJ mol^{-1}) is within error of the theory level employed. Nonetheless we speculate that owing to steric repulsion derived from close proximity between the reaction center (C1) and $Yb(OTf)_3$(EG) on C2 group, the 1,4-dehydration introduces a larger energy barrier. Possibly due to this reason, the addition of $Yb(OTf)_3$ facilitates the 3,6-dehydration at C6 over the 1,4- and 1,5-dehydration at C1.

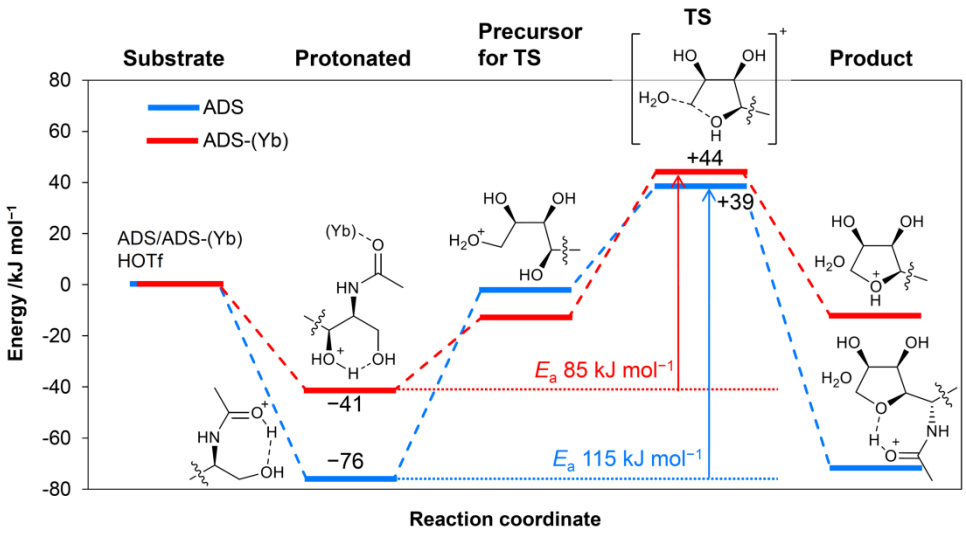

Figure 5. Energy diagrams for the 3,6-dehydration of ADS. (Yb) indicates $Yb(OTf)_3$(EG). Energy contains electronic and zero-point vibration energies.

4. Conclusions

We conducted the dehydration reaction of ADS in the presence of Brønsted acid and Lewis acid catalysts. The combination of HOTf and $Yb(OTf)_3$ gives 40% yield of ADI at 60 min, which is superior to the HOTf-only system (32% yield of ADI at 180 min). $Yb(OTf)_3$ plays two roles in this reaction: first, the acceleration of dehydration reactions to produce ADI, which shortens the reaction time by one third. $Yb(OTf)_3$ coordinates the amide groups of substrates, which prevents the neutralization of protons by the amide groups. DFT calculations have revealed that the apparent activation energy decreases by 30 kJ mol^{-1} by this manner. The other role is the selectivity change toward the dehydration at C6 position (3,6-dehydration) over that at C1 position (1,4- and 1,5-dehydration). This is useful to reduce the formation of 1,5-anhydro-ADS, a major by-product, thus leading to a slightly higher yield of ADI. We propose that coordination of the bulky Yb complex at amide position possibly increases the steric hindrance for the dehydration reactions at C1. Hence, our method directs toward overcoming the major issues present in the dehydration of ADS to ADI, and these insights would be applicable for the development of efficient catalytic systems for acid-catalyzed reactions of amide-containing molecules.

CRediT authorship contribution statement

Takuya Sagawa: Conceptualization, Data curation, Formal analysis, Investigation, Writing – Original draft preparation, Visualization, Funding acquisition. **Hirokazu Kobayashi:** Conceptualization, Methodology, Validation, Formal analysis, Resources, Writing – Review & editing, Visualization, Supervision, Funding acquisition. **Atsushi Fukuoka:** Resources, Writing – Review & editing, Supervision, Funding acquisition.

Acknowledgements

This work was supported by a Grant-in-Aid for Scientific Research (B) (No. 18H01781) and a Grant-in-Aid for Young Scientists (No. 19K15608) from the Japan Society for the Promotion of Science (JSPS) and by the Japan Science and Technology Agency (JST) ALCA (Project No. JPMJAL1309). We utilized NMR spectrometers at the Open Facility of Institute for Catalysis (ICAT), Hokkaido University.

References

[1] K. Kurita, Chitin and Chitosan: Functional Biopolymers from Marine Crustaceans, Mar. Biotechnol. 8 (2006) 203−226. https://doi.org/10.1007/s10126-005-0097-5

[2] J. Chen, C. Shen, C. Liu, *N*-Acetylglucosamine: Production and Applications, Mar. Drugs 8 (2010) 2493−2516. https://doi.org/10.3390/md8092493

[3] M. Yabushita, H. Kobayashi, K. Kuroki, S. Ito, A. Fukuoka, Catalytic Depolymerization of Chitin with Retention of *N*-Acetyl Group, ChemSusChem 8 (2015) 3760−3763. https://doi.org/10.1002/cssc.201501224

[4] H. Kobayashi, K. Techikawara, A. Fukuoka, Hydrolytic hydrogenation of chitin to amino sugar alcohol, Green Chem. 19 (2017) 3350−3356. https://doi.org/10.1039/C7GC01063J

[5] J. G. Zhang, N. Yan, A Robust Ru/ZSM-5 Hydrogenation Catalyst: Insights into the Resistances to Ruthenium Aggregation and Carbon Deposition, ChemCatChem 9 (2017) 2790−2796. https://doi.org/10.1002/cctc.201700664

[6] N. Yan, X. Chen, Sustainability: Don't waste seafood waste, Nature 524 **(**2015) 155−157. http://doi.org/10.1038/524155a

[7] X. Ma, G. Gözaydın, H. Yang, W. Ning, X. Han, N. Y. Poon, H. Liang, N. Yan, K. Zhou, Upcycling chitin-containing waste into organonitrogen chemicals via an integrated process, Proc. Natl. Acad. Sci. USA 117 (2020) 7719−7728. https://doi.org/10.1073/pnas.1919862117

[8] A. Shrotri, H. Kobayashi, A. Fukuoka, Catalytic Conversion of Structural Carbohydrates and Lignin to Chemicals, C. Song (Eds.), Advances in Catalysis, Vol. 60, Elsevier, 2017, pp. 59−123.

[9] X. Chen, H. Yang, N. Yan, Shell Biorefinery: Dream or Reality?, Chem. Eur. J. 22 (2016) 13402−13421. https://doi.org/10.1002/chem.201602389

[10] W. Deng, Y. Wang, S. Zhang, K. M. Gupta, M. J. Hülsey, H. Asakura, L. Liu, Y. Han, E. M. Karp, G. T. Beckham, P. J. Dyson, J. Jiang, T. Tanaka, Y. Wang, N. Yan, Vitrification is essential for

anhydrobiosis in an African chironomid, *Polypedilum vanderplanki*, Proc. Natl. Acad. Sci. USA 115 (2018) 5093−5098. https://doi.org/10.1073/pnas.0706197105

[11] Y. S. Nakagawa, Y. Oyama, N. Kon, M. Nikaido, K. Tanno, J. Kogawa, S. Inomata, A. Masui, A. Yamamura, M. Kawaguchi, Y. Matahira, K. Totani, Development of innovative technologies to decrease the environmental burdens associated with using chitin as a biomass resource: Mechanochemical grinding and enzymatic degradation, Carbohydr. Polym. 83 (2011) 1843−1849. https://doi.org/10.1016/j.carbpol.2010.10.050

[12] M. Osada, K. Kikuta, K. Yoshida, K. Totani, M. Ogata, T. Usui, Non-catalytic synthesis of Chromogen I and III from *N*-acetyl-d-glucosamine in high-temperature water, Green Chem. 15 (2013) 2960−2966. https://doi.org/10.1039/C3GC41161C

[13] Y. Pierson, X. Chen, F. D. Bobbink, J. Zhang, N. Yan, Acid-Catalyzed Chitin Liquefaction in Ethylene Glycol, ACS Sustainable Chem. Eng. 2 **(**2014) 2081−2089. https://doi.org/10.1021/sc500334b

[14] F. D. Bobbink, J. Zhang, Y. Pierson, X. Chen, N. Yan, Conversion of chitin derived *N*-acetyl-d-glucosamine (NAG) into polyols over transition metal catalysts and hydrogen in water, Green Chem. 17 (2015) 1024−1031. https://doi.org/10.1039/C4GC01631A

[15] K. Techikawara, H. Kobayashi, A. Fukuoka, Conversion of *N*-Acetylglucosamine to Protected Amino Acid over Ru/C Catalyst, ACS Sustainable Chem. Eng. 6 (2018) 12411−12418. https://doi.org/10.1021/acssuschemeng.8b02951

[16] G. Margoutidis, V. H. Parsons, C. S. Bottaro, N. Yan, F. M. Kerton, Mechanochemical Amorphization of α-Chitin and Conversion into Oligomers of *N*-Acetyl-d-glucosamine, ACS Sustainable Chem. Eng. 6 (2018) 1662−1669. https://doi.org/10.1021/acssuschemeng.7b02870

[17] A. D. Sadiq, X. Chen, N. Yan, J. Sperry, Towards the Shell Biorefinery: Sustainable Synthesis of the Anticancer Alkaloid Proximicin A from Chitin, ChemSusChem 11 (2018) 532−535. https://doi.org/10.1002/cssc.201702356

[18] T. T. Pham, X. Chen, T. Söhnel, N. Yan, J. Sperry, Oxidative Ring-Expansion of a Chitin-Derived Platform Enables Access to Unexplored 2 ‐ Amino Sugar Chemical Space, Eur. J. Org. Chem. 6 (2019) 1355−1360. https://doi.org/10.1002/ejoc.201801683

[19] T. T. Pham, X. Chen, T. Söhnel, N. Yan, J. Sperry, Haber-independent, diversity-oriented synthesis of nitrogen compounds from biorenewable chitin, Green Chem. 22 (2020) 1978−1984. https://doi.org/10.1039/D0GC00208A

[20] T. Sagawa, H. Kobayashi, C. Murata, Y. Shichibu, K. Konishi, A. Fukuoka, Catalytic Conversion of a Chitin-Derived Sugar Alcohol to an Amide-Containing Isosorbide Analog, ACS Sustainable Chem. Eng. 7 (2019) 14883–14888. https://doi.org/10.1021/acssuschemeng.9b02985

[21] T. Setoyama, The Contribution of Catalysis for the Realization of GSC in the Twenty-First Century, Catal. Surv. Asia 18 (2014) 183−192. http://dx.doi.org/10.1007/s10563-015-9188-0

[22] S. Kobayashi, Rare Earth Metal Trifluoromethanesulfonates as Water-Tolerant Lewis Acid Catalysts in Organic Synthesis, Synlett 9 (1994) 689–701. http://doi.org/10.1055/s-1994-22976

[23] J. Becica, G. E. Dobereiner, Acceleration of Pd-Catalyzed Amide N-Arylations Using Cocatalytic Metal Triflates: Substrate Scope and Mechanistic Study, ACS Catal. 7 **(**2017) 5862–5870. https://doi.org/10.1021/acscatal.7b01317

[24] R. Zhu, J. Jiang, K. Li, J. Deng, Y. Fu, A Comprehensive Study on Metal Triflate-Promoted Hydrogenolysis of Lactones to Carboxylic Acids: From Synthetic and Mechanistic Perspectives, ACS Catal. 7, (2017) 7520–7528. https://doi.org/10.1021/acscatal.7b01569

[25] H. Yokoyama, H. Kobayashi, J. Hasegawa, A. Fukuoka, Selective Dehydration of Mannitol to Isomannide over Hβ Zeolite, ACS Catal. 7, (2017) 4828–4834. https://doi.org/10.1021/acscatal.7b01295

[26] A. Yamaguchi, N. Mimura, M. Shirai, O. Sato, Kinetic analyses of intramolecular dehydration of hexitols in high-temperature water, Carbohydr. Res. 487 (2020) 107880. https://doi.org/10.1016/j.carres.2019.107880

[27] W. J. Hehre, R. Ditchfield, J. A. Pople, Self-Consistent Molecular Orbital Methods. XII. Further Extensions of Gaussian-Type Basis Sets for Use in Molecular Orbital Studies of Organic Molecules, J. Chem. Phys. 56 (1972) 2257−2261. https://doi.org/10.1063/1.1677527

[28] C. Lee, W. Yang, R. G. Parr, Development of the Colle-Salvetti correlation-energy formula into a functional of the electron density, Phys. Rev. B: Condens. Matter Mater. Phys. 37 (1988) 785−789. https://doi.org/10.1103/PhysRevB.37.785

[29] A. D. Becke, Density‐functional thermochemistry. III. The role of exact exchange, J. Chem. Phys. 98 (1993) 5648−5652. https://doi.org/10.1063/1.464913

[30] F. Weigend, R. Ahlrichs, Balanced basis sets of split valence, triple zeta valence and quadruple zeta valence quality for H to Rn: Design and assessment of accuracy, Phys. Chem. Chem. Phys. 7 (2005) 3297−3305. https://doi.org/10.1039/B508541A

[31] A. V. Marenich, C. J. Cramer, D. G. Truhlar, Universal Solvation Model Based on Solute Electron Density and on a Continuum Model of the Solvent Defined by the Bulk Dielectric Constant and Atomic Surface Tensions, J. Phys. Chem. B 113 (2009) 6378−6396. https://doi.org/10.1021/jp810292n

[32] M. Mammen, E. I. Shakhnovich, J. M. Deutch, G. M. Whitesides, Estimating the Entropic Cost of Self-Assembly of Multiparticle Hydrogen-Bonded Aggregates Based on the Cyanuric Acid·Melamine Lattice, J. Org. Chem. 63 (1998) 3821−3830. https://doi.org/10.1021/jo970944f

[33] Y. Izato, A. Matsugi, M. Koshi, A. Miyake, A simple heuristic approach to estimate the thermochemistry of condensed-phase molecules based on the polarizable continuum model, Phys. Chem. Chem. Phys. 21 (2019) 18920−18929. https://doi.org/10.1039/C9CP03226F

[34] K. Fukui, Formulation of the reaction coordinate, J. Phys. Chem. 74 (1970) 4161−4163. https://doi.org/10.1021/j100717a029

[35] H. Tsuruta, K. Yamaguchi, T. Imamoto, Evaluation of the relative Lewis acidities of lanthanoid(III) compounds by tandem mass spectrometry, Chem. Commun. (1999) 1703−1704. https://doi.org/10.1039/A905569J

[36] J. M. Harrowfield, D. L. Kepert, J. M. Patrick, A. H. White, Structure and stereochemistry in 'f-block' complexes of high coordination number. VIII. The [M(unidentate)$_9$] system. Crystal structures of [M(OH_2)$_9$] [CF_3SO_3]$_3$, M = La, Gd, Lu, Y, Aust. J. Chem. 36 (1983) 483−492. https://doi.org/10.1071/CH9830483

[37] S. J. Butler, M. Delbianco, L. Lamarque, B. K. McMahon, E. R. Neil, R. Pal, D. Parker, J. W. Walton, J. M. Zwier, EuroTracker® dyes: design, synthesis, structure and photophysical properties of very bright europium complexes and their use in bioassays and cellular optical imaging, Dalton Trans. 44 (2015) 4791−4803. https://doi.org/10.1039/C4DT02785J

[38] T. Madanhire, H. Davids, M. C. Pereira, E. C. Hosten, A. Abrahams, Synthesis, characterisation and anticancer activity screening of lanthanide(III) acetate complexes with benzohydrazone and nicotinohydrazone ligands, Polyhedron 184 (2020) 114560. https://doi.org/10.1016/j.poly.2020.114560

Graphical abstract

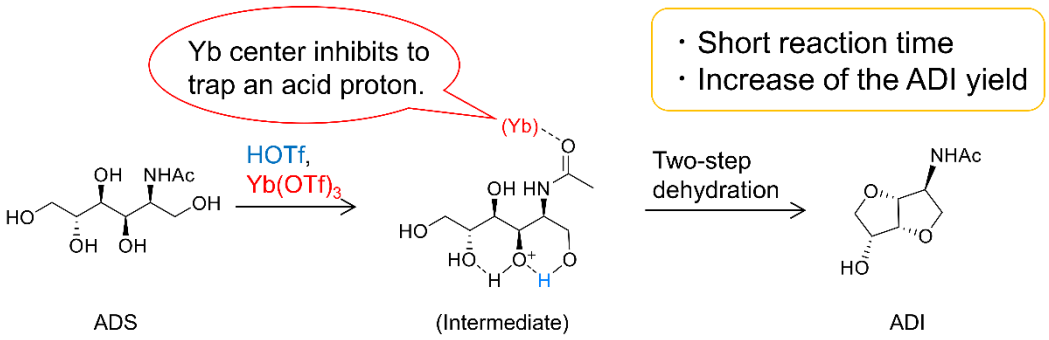

Figure Captions

Figure 1. Synthetic route of ADI from chitin.

Figure 2. Gibbs free energies for coordination of ADS on $Yb(OTf)_3(EG)$ estimated by the DFT calculations.

Figure 3. Time courses of ADS dehydration reactions at 150 °C: (a) in the absence of $Yb(OTf)_3$, (b) an enlarged image of (a), (c) in the presence of $Yb(OTf)_3$, (d) an enlarged image of (c).

Figure 4. Protonation energies for ADS and sorbitol. The value includes electronic energy and zero-point vibration energy. (Yb) in structures indicates $Yb(OTf)_3(EG)$.

Figure 5. Energy diagrams for the 3,6-dehydration of ADS. (Yb) indicates $Yb(OTf)_3(EG)$. Energy contains electronic and zero-point vibration energies.